Optimum Order of Angle Diversity With Equal-Gain Combining Receivers for Broad-Band Indoor Optical Wireless Communications

Yazan A. Alqudah and Mohsen Kavehrad, *Fellow, IEEE*

***Abstract*—Angle diversity is an effective technique to compensate for multipath temporal dispersion in a wireless infrared environment. Diversity is accomplished by using a multibranch receiver capable of resolving multipath. The goal of this paper is to illustrate the effect that the increasing diversity order of a receiver has on the performance of a link in a multispot-diffusing configuration with equal-gain combining outage probability based on probability of bit error is adopted as a performance measure. It is shown that there is an optimal number of branches, which minimizes outage probability. Increasing diversity order beyond this optimal number degrades the performance and increases the receiver complexity, cost, and susceptibility to any shadowing effects.**

***Index Terms*—Angle diversity, receiver design, temporal dispersion.**

I. Introduction

OPTICAL [infrared (IR)] wireless local-access links provide an attractive alternative to radio-frequency (RF) links. A large unregulated bandwidth along with a spatial confinement of IR propagation provides an abundance of bandwidth and the opportunity to reuse this band for broad-(band wireless local-access applications.

Optical wireless links can be classified according to the directivity of a transmitter and a receiver and whether a line of sight (LoS) exists between the transmitter and receiver [1]. Unlike RF transmission, both narrow- and wide-angle IR communications can support high data rates, but at a cost. Narrow-angle transmission requires precise alignment of transmitter and receiver, while wide-angle transmission demands a high power level. In [2], a novel configuration was proposed called multispot diffusing configuration (MSDC). This model combines elements of both narrow- and wide-angle systems to deliver high data rates with low power. In this configuration, a multibeam transmitter is used to distribute the optical power within a room, uniformly. Angle diversity is used at the receiver to combat the induced multipath temporal dispersion and background noise. The MSDC concept was further investigated in [3]–[16].

This paper investigates angle diversity at the receiver, with the objective of determining the optimal number of branches needed under MSD configurations, thus reducing receiver cost and complexity. Reducing the number of branches also reduces shadowing effect, which occurs when signal paths to branches are obstructed by an object. Outage probability is used as a measure of link quality for different receiver parameters.

This paper is organized as follows. In Section II, the maximum number of achievable angle-diversity channels is calculated at the receiver. Section III introduces a model of the IR link with diversity, under the assumption that diversity channels can be made ideal, using more complex receivers. In Section IV, the ideal model is revised to account for the inability of angle diversity to remove all multipath dispersion, using simpler receivers. Section V provides expressions for the performance measures used in the computer simulations. Simulation results are presented in Section VI. Concluding remarks are presented in Section VII.

II. Available Diversity Channels

A multibranch receiver is composed of several branches (photodiodes). In this section, we describe a packing method that maximizes nonoverlapping branches that can encompass an entire (total) receiver field of view (FOV) $\mathrm{FOV}_{\mathrm{total}}$. This number represents the maximum degree of diversity $L_{\max}$ that can be achieved. To help visualize branches arrangement, a hypothetical sphere of unit radius is assumed to surround a receiver placed at its center. Each branch has a circular footprint on the sphere surface. The footprint represents the area on the sphere surface that falls within the branch FOV $(\mathrm{FOV}_{\mathrm{branch}})$. New branches are added such that the centers of these circles are situated on a ring with an increasing radius around the central branch. The number of branches in a given ring is evaluated with the aid of Fig. 1 and is given by $\lfloor \pi \sin(2 \times n \times \mathrm{FOV}_{\mathrm{branch}}(\mathrm{rad}))/\mathrm{FOV}_{\mathrm{branch}}(\mathrm{rad}) \rfloor$. In this expression, n is the ring index with a central branch having index $= 0$, $\lfloor x \rfloor$ denotes the maximum integer smaller or equal to x. Given $\mathrm{FOV}_{\mathrm{total}}$ and $\mathrm{FOV}_{\mathrm{branch}}$, the total number of achievable branches is

$$L_{\max} = 1 + \sum_{n=1}^{V} \left\lfloor \frac{\pi \times \sin(2 \times n \times \mathrm{FOV}_{\mathrm{branch}})}{\mathrm{FOV}_{\mathrm{branch}}(\mathrm{rad})} \right\rfloor \quad (1)$$

where $V = \lfloor (\mathrm{FOV}_{\mathrm{total}} - \mathrm{FOV}_{\mathrm{branch}})/(2 \times \mathrm{FOV}_{\mathrm{branch}}) \rfloor$ is the total number of rings surrounding the central branch. For example, if $\mathrm{FOV}_{\mathrm{total}} = 34.5°$ and $\mathrm{FOV}_{\mathrm{branch}} = 11.5°$, the maximum diversity order is 7. The number of branches does not linearly depend on $\mathrm{FOV}_{\mathrm{total}}$, nor is there a $\mathrm{FOV}_{\mathrm{total}}$ for every number of branches. This is further demonstrated in Table I,

Manuscript received July 23, 2002; revised March 25, 2003, August 11, 2003, October 5, 2003, and October 17, 2003.

The authors are with the Center for Information and Communications Technology Research (CICTR), Department of Electrical Engineering, The Pennsylvania State University, University Park, PA 16802 USA (e-mail: mkavehrad@psu.edu).

Digital Object Identifier 10.1109/TVT.2003.822023

0018-9545/04$20.00 © 2004 IEEE

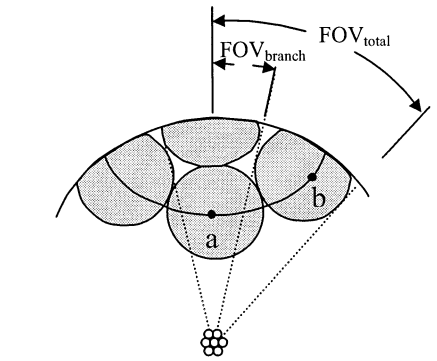

$$2r_f = FOV_{branch}(rad)$$
$$r_r = \sin(FOV_{total} - FOV_{branch})$$

(a)

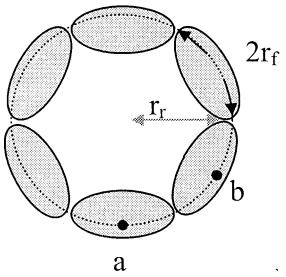

(b)

Fig. 1. (a) Footprints of multibranch receiver on a hypothetical sphere of unit radius. The receiver is placed at the sphere center. (b) Top view of the footprint at ring index = 1.

TABLE I
AVAILABLE $\mathrm{FOV_{total}}$ FOR DIFFERENT NUMBER OF BRANCHES

Number of Branches	$\mathrm{FOV_{total}}$	
	$\mathrm{FOV_{branch}}$=7°	$\mathrm{FOV_{branch}}$=11.5°
1	7°	11.5°
7	21°	34.5°
18		57.5°
19	35°	
32		82.5°
36	49°	

where available $\mathrm{FOV_{total}}$ for two different $\mathrm{FOV_{branch}}$ values and different number of branches are provided. Using number of branches that fills the entire ring provides rotational symmetry at the receiver. If a different number of branches is used, the behavior of the receiver will depend upon the arrangement of branches, thus rotating the receiver changes its behavior.

III. CHANNEL AND NOISE MODELS

This section describes the environment and introduces an equivalent mathematical model for the IR communication system with a diversity receiver. An empty room with the dimensions of 6 m×6 m×3 m is considered. The multibeam transmitter is placed in the center of the room to produce a 10 × 10 equal-intensity diffusing spots grid on the ceiling [8].

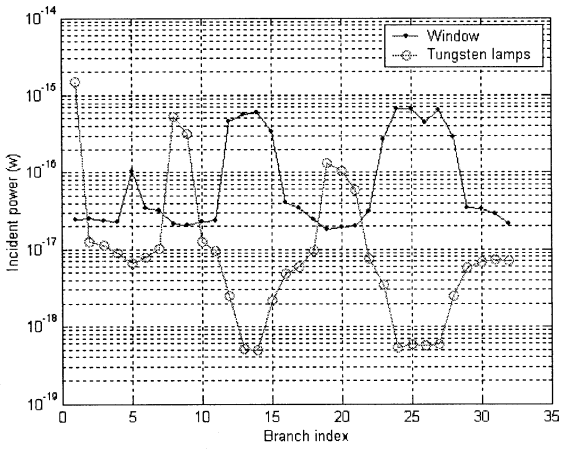

Fig. 2. Incident optical power distribution of a receiver composed of 32 branches $\mathrm{FOV_{branch}} = 11.5°$. Branches facing a window or lamps experience a higher incident power.

The ceiling and walls are modeled as Lambertian reflectors of the first order [1]. More about the environment parameters is presented in the computer simulation results of Section VI.

A. Noise Model

The main degradation of a wireless optical link is caused by ambient light. Unlike as in fiber communications, a wireless link has to contend with ambient light coming from the sun through windows, light from lighting fixtures, and other sources of artificial light. The photocurrent generated in response to ambient light results in current fluctuations and the latter are attributed to shot noise. Current fluctuations are characterized by a stationary random process with Poisson statistics that can, in practice, be approximated by Gaussian statistics [17], [18]. The two-sided spectral density of shot noise at the output of the photodiode is a constant given by

$$S(f) = q\,I_{bg} = q\,RP_{bg}. \tag{2}$$

In (2), R is the detector responsivity (A/W), q is an electron charge (C), I_{bg} is photocurrent (A), and P_{bg} is the incident optical power (W). The ambient light herein results from a window in the room and nine Tungsten lamps on the ceiling. To calculate the incident optical power, the window surface is divided into small elements of area equal to 0.04 m^2 and each element is modeled as a first-order Lambertian source. The lamps are also modeled as Lambertian sources of second order.

Noise spectral density depends upon the receiver location and branch orientation relative to the light sources. A higher current is generated when a receiver branch falls within the LoS of a light source. Fig. 2 shows the variation of incident optical power for a typical 32-branch receiver.

The variance of noise at the output of a receiver that incorporates a receive filter $G(f)$is given by

$$\sigma^2 = 2qI_{bg}\int_0^\infty |G(f)|^2\,df. \tag{3}$$

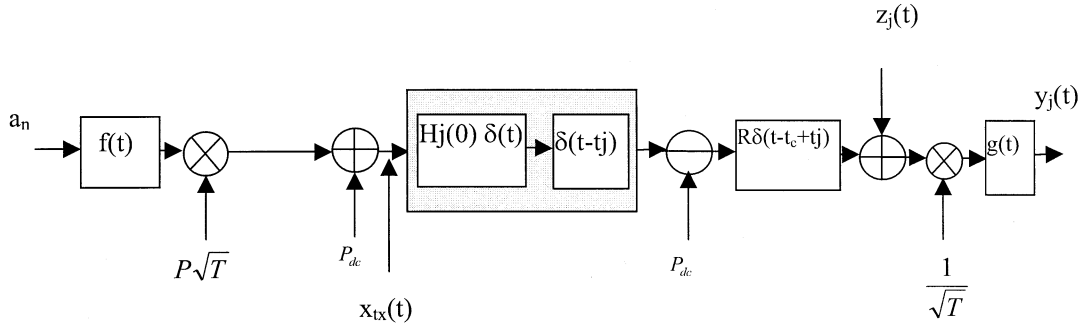

Fig. 3. jth channel with an angle-diversity receiver.

B. Channel Model

The transmission link in this paper uses intensity modulation and direct detection (IM/DD), with ON–OFF keying modulation. In deriving the channel model, it is first assumed that the channel to each branch can be modeled as an ideal channel, with no temporal dispersion. This assumption is not necessarily true in general, as will be explained in the next section, where the channel model is modified to account for a residual temporal dispersion. Each channel is modeled as an additive Gaussian one, using a constant gain and a constant delay. Gain of the jth branch is equal to $H_j(0)$ and the delay is equal to t_j. Channel gain can be zero, indicating that no signal is received through the branch. The noise terms in the L channels are assumed to be mutually statistically independent. The transmitter and receiver filters are identical, each accomplishing half the signal shaping. The jth channel is shown in Fig. 3.

The receiver compensates for the delay that a signal experiences, while passing through the channel. It also adds delay t_c to the signal in order to ensure causality of the receiver filter, i.e., $t_c \geq \max[t_i]$, $i \in \{1, L\}$. A factor R at the receiver is added due to the photo-detector responsivity. Since noise spectral density is flat and transmission channel is real, the transmitter and receiver filters that eliminate intersymbol interference and maximize the signal-to-noise ratio (SNR) at sampling time, for a given input power, follow from [14], [19] as

$$F(f)G(f) = X_{rc}(f) \tag{4}$$

where X_{rc} is a raised cosine frequency response, $F(f)$ and $G(f)$ are transmitter and receiver filters, respectively. The filters magnitude is given by

$$|F(f)| = |G(f)| = \sqrt{|X_{rc}(f)|}. \tag{5}$$

Therefore, both $f(t)$ and $g(t)$ have root-raised cosine with a time-domain representation from [20] as

$$f(t) = g(t) = \frac{4\alpha}{\pi\sqrt{T}} \frac{\cos\left[(1+\alpha)\frac{\pi t}{T}\right] + \frac{\sin\left[(1-\alpha)\left(\frac{\pi t}{T}\right)\right]}{\left[\frac{4\alpha t}{T}\right]}}{1 - \left(\frac{4\alpha t}{T}\right)^2} \tag{6}$$

where α is the roll-off factor and T is the time separation between successive pulses. Two observations are needed with regard to the root-raised cosine waveform, when channel constraints are arrived at. First, the maximum value of $f(t)$ is

$$\max(f(t)) = f(0) = \frac{1}{\sqrt{T}}\left(1 - \alpha + \frac{4\alpha}{\pi}\right). \tag{7}$$

Second, the average value of a sequence of pulses that are shaped by $f(t)$, i.e., $\sum_{n=-N}^{N} f(t - nT)$, is

$$\lim_{NT\to\infty} \frac{1}{2NT} \int_{-NT}^{NT} \sum_{n=-N}^{N} f(t - nT)dt = \frac{1}{T}\int_{-\infty}^{\infty} f(t)dt = \frac{F(0)}{T} = \frac{\sqrt{X_{rc}(0)}}{T} = \frac{1}{\sqrt{T}}. \tag{8}$$

Substituting for $G(f)$ in (3), the noise variance at the output of $g(t)$ becomes

$$\begin{aligned}\sigma^2 &= 2qI_{bg} \times \left(\frac{1}{\sqrt{T}}\right)^2 \int_0^{\infty} |G(f)|^2\, df \\ &= 2qI_{bg} \times \frac{1}{T} \times \frac{1}{2} \times \int_{-\infty}^{\infty} X_{rc}(f)df \\ &= qI_{bg}B \\ &= qRP_{bg}B\end{aligned} \tag{9}$$

where B is the bit rate and is equal to $1/T$.

C. Channel Constraints

In IM/DD, the transmitted signal $x_{tx}(t)$ represents optical intensity. This leads to two constraints on $x_{tx}(t)$ [1]. First, the value of $x_{tx}(t)$ must be nonnegative. Second, the average amplitude of $x_{tx}(t)$ must be kept below a specified value P_m, determined by the power consumption and eye safety limits. These constraints can be expressed as

$$x_{tx}(t) \geq 0 \tag{10}$$

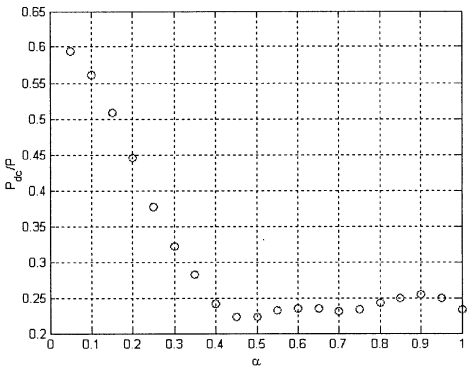

(a)

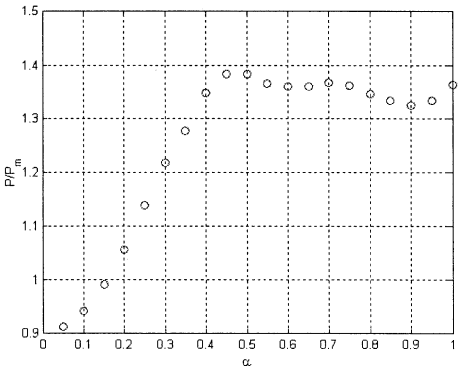

(b)

Fig. 4. (a) P_{dc}/P as α function of (b) maximum normalized power P/P_m versus α.

and

$$\lim_{T\to\infty}\frac{1}{2\tau}\int_{-\tau}^{\tau}x_{tx}(t)dt \le P_m. \tag{11}$$

To determine the parameters of $x_{tx}(t)$ that satisfy these constraints, $x_{tx}(t)$ is expressed as [14]

$$x_{tx}(t) = P_{dc} + P\sqrt{T}\sum_{n=-N}^{N} a_n f(t-nT) \tag{12}$$

where $2N+1$ is transmitted sequence length and $P_{\rm dc}$ term is added to ensure that $x_{tx}(t)$ is positive. The value of $P_{\rm dc}$ is equal in magnitude to the minimum of $P\sqrt{T}\sum_{n=-N}^{N} a_n f(t-nT)$. If $\lambda(\alpha) = \text{abs}(\min(\sum_{\rm n=-N}^{N} a_n f(t-nT))/\max(f(t)))$ is defined, $P_{\rm dc}$ can be expressed as

$$\begin{aligned} P_{\rm dc} &= P\sqrt{T}\times\lambda(\alpha)\times\max\left(f(t)\right)\\ &= P\times\lambda(\alpha)\times\left(1-\alpha+\frac{4\alpha}{\pi}\right). \end{aligned} \tag{13}$$

The value of λ is found by considering different sequences of transmitted symbols a_n and finding the minimum of $x_{tx}(t)$. Since $f(t)$ is a decaying function of time, a sequence of 12 symbols is used to generate the plot in Fig. 4(a). The figure shows that for small values of α, as α increases, $P_{\rm dc}$ decreases.

The second constraint is used to determine the scaling factor P. Assuming that input symbols are equally likely to be 0 and $+1$, the average value of $x_{tx}(t)$, for very large value of N, is given by

$$\begin{aligned} \lim_{\tau\to\infty}\frac{1}{2\tau}\int_{-\tau}^{\tau}x_{tx}(t)dt &= P_{\rm dc} + P\sqrt{T}\times E[a_n]\times\frac{1}{\sqrt{T}}\\ &= P_{\rm dc}+\frac{P}{2}. \end{aligned} \tag{14}$$

Substituting for $P_{\rm dc}$, we obtain

$$\lambda\times\left(1-\alpha+\frac{4\alpha}{\pi}\right)\times P+\frac{P}{2}\le P_m. \tag{15}$$

Expressing P in terms of P_m

$$P\le\frac{P_m}{\left[0.5+\lambda(\alpha)\times\left(1-\alpha+\frac{4\alpha}{\pi}\right)\right]}. \tag{16}$$

Equation (16) provides the maximum amplitude the signal can take on when its average is constrained to be less than P_m. The relationship between P and P_m as a function of α is depicted in Fig. 4(b). The figure shows that for small values of α, any increase in α will cause an increase in P. The value of P reaches a maximum when α is close to 0.5. Increasing α beyond 0.5 has a very little effect on P.

It is worth mentioning that $P_{\rm dc}$ carries no information and is subtracted from the signal at the receiver. This explains why it is desirable to have a pulse shape that has a small $P_{\rm dc}$ value.

D. Receiver Output

The receiver, in an angle-diversity system, is composed of L branches, each of which contains a filter matching the received waveform and a delay that depends on the channel. To calculate the receiver output, an equivalent channel impulse response $h_{\rm eq}(t)$ is defined as

$$h_{\rm eq}(t) = \sum_{i=1}^{L} H_i(0)\delta(t). \tag{17}$$

In terms of $h_{\rm eq}$, the output is expressed as

$$y(t) = \text{RP}\sum_{n=-N}^{N} a_n f(t-nT)\otimes h_{\rm eq}(t)\otimes g(t-t_c) \tag{18}$$

where $2N+1$ is a transmitted sequence length. Substituting for $h_{\rm eq}(t)$ and using (4), the expression for $y(t)$ becomes

$$y(t) = \text{RP}\sum_{n=-N}^{N} a_n\sum_{i=1}^{L} H_i(0)x_{\rm rc}(t-nT-t_c). \tag{19}$$

The noise at the output of the receiver is equal to the summation of noise at the output of each channel. At the output of the

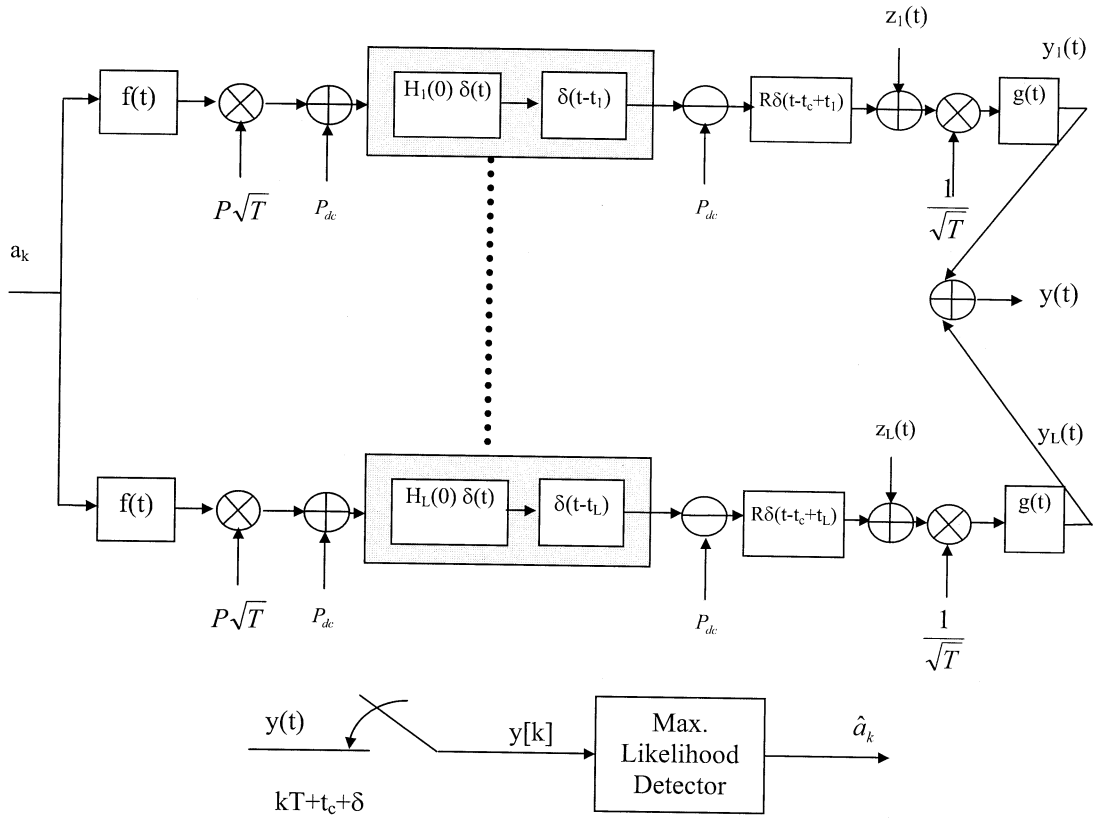

Fig. 5. Multibranch angle-diversity receiver, using equal-gain combining.

ith receiver, the noise $z_i(t)$ is a zero-mean Gaussian term. The expression for the output $y(t)$, including the noise, becomes

$$y(t) = \mathrm{RP} \sum_{n=-N}^{N} \sum_{i=1}^{L} a_n H_i(0) x_{\mathrm{rc}}(t - nT - t_c) + \sum_{i=1}^{L} z_i(t). \tag{20}$$

The output $y(t)$ is sampled at time $t_{\mathrm{sampling}} = t_c + \delta + kT$, where δ is a time delay chosen to minimize intersymbol interference when the channel is not ideal (dispersion free), as discussed in the next section. Thus, $y[k]$ is

$$\begin{aligned} y[k] &= y[t_s + \delta + kT] \\ &= \mathrm{RP} \sum_{n=-N}^{N} \sum_{i=1}^{L} a_n H_i(0) x_{\mathrm{rc}}(kT - nT + \delta) \\ &\quad + \sum_{i=1}^{L} z_i(kT + t_c + \delta). \end{aligned} \tag{21}$$

In this subsection, channels are assumed dispersionless (ideal); therefore, $\delta = 0$. Since $x_{\mathrm{rc}}(nT) = 0, \forall\, n \neq 0$, (21) simplifies to

$$y[k] = \mathrm{RP} \sum_{i=1}^{L} a_k H_i(0) + \eta \tag{22}$$

where variance of noise η is found by summing noise variance over all channels, i.e.,

$$\sigma_\eta^2 = \sum_{i=1}^{L} \sigma_i^2. \tag{23}$$

A maximum likelihood receiver uses the sampled output $y[k]$ to decide which symbol is transmitted. Assuming the 0 and 1 are equally likely to occur, the detected symbol $\hat{a}_k$ is determined according to

$$\hat{a}_k = \left\{ \begin{matrix} 1, \text{ if } P\left(y[k] | a_k = 1\right) > P\left(y[k] | a_k = 0\right) \\ 0, \text{ if } P\left(y[k] | a_k = 0\right) < P\left(y[k] | a_k = 1\right) \end{matrix} \right\}. \tag{24}$$

The multibranch equal gain receiver is illustrated in Fig. 5.

E. Performance Measures

Two measures are used to evaluate the outage performance of the receiver and to determine the optimal number of branches: the probability of error and SNR, which are not independent of one another. For a maximum likelihood detector, assuming symbols are equally likely to be 0 or 1, the probability of error is

$$P_e = Q\left(\frac{P \sum_{i=1}^{L} \frac{\mathrm{RH}_i(0)}{2}}{\sqrt{\sum_{i=1}^{L} \sigma_i^2}} \right) \tag{25}$$

where $Q(.)$ is a Q-function defined as $(1/\sqrt{2\pi})\int_x^\infty \exp(-(1/2)u^2)du$, $u \geq 0$. The SNR is defined as the ratio of the output signal power when $a_n = 1$ is transmitted to the noise power and is equal to

$$\mathrm{SNR} = \frac{\left(P\sum_{i=1}^{L}\mathrm{RH}_i(0)\right)^2}{\sum_{i=1}^{L}\sigma_i^2}. \tag{26}$$

Expressed in terms of SNR, the probability of error is

$$P_e = Q\left(\frac{\sqrt{\mathrm{SNR}}}{2}\right). \tag{27}$$

Eqs. (25) and (26) highlight the dependence of error probability on the number of channels. Increasing the number of channels increases the noise, but does not necessarily increase the SNR value. This is because some of the newly added branches might have $H_i(0)$ equal to zero or a very small value compared to added noise.

IV. More Accurate Channel Model

The assumption made in the previous section about the ability of diversity receiver to eliminate temporal dispersion may not apply to all indoor IR transceivers. For example, with equal-gain combining considered herein, there are two circumstances under which temporal dispersion may not be eliminated completely. The first occurs when the $\mathrm{FOV_{branch}}$ is larger than a critical angle $\mathrm{FOV_{critical}}$. In this case, the branch spans more than a single diffusing spot. This results in an impulse response that is made of at least two impulses. Added delay at a simple combining receiver can only align one of these impulses.

The value of $\mathrm{FOV_{critical}}$ depends upon the receiver location relative to the diffusing spots. To guarantee the elimination of temporal dispersion throughout the room, the worst receiver location is considered. This location is close to the corner of the room, as illustrated in Fig. 6. From this figure

$$\begin{aligned} x &= h\times\tan(\mathrm{FOV_{total}}),\\ \tan(\mathrm{FOV_{total}}-2\times\mathrm{FOV_{branch}}) &= \frac{x-d}{h}\\ \mathrm{FOV_{critical}} &= \frac{1}{2}\times\left[\mathrm{FOV_{total}} - \arctan\left(\frac{h\times\tan(\mathrm{FOV_{total}})-d}{h}\right)\right] \end{aligned} \tag{28}$$

where x is the distance to the farthest spot that lies within $\mathrm{FOV_{total}}$, h is the distance from receiver to the surface containing spots, and d is the spacing between spots. For example, for $\mathrm{FOV_{total}} = 34.5°$, $h = 2.1\ m$, and $d = 0.6\ m$, the $\mathrm{FOV_{critical}} = 6.3°$.

The second case that lends itself to a dispersive channel mode, considering signals received after reflection off of walls and ceiling, as illustrated in Fig. 7. Since the signal strength at the receiver is inversely proportional to the square of traveled distance by light and walls do not offer perfect reflection, dispersion caused by reflections contributes smaller components to channel-impulse response. This dispersion is reduced by reducing the $\mathrm{FOV_{branch}}$, but may not be completely eliminated.

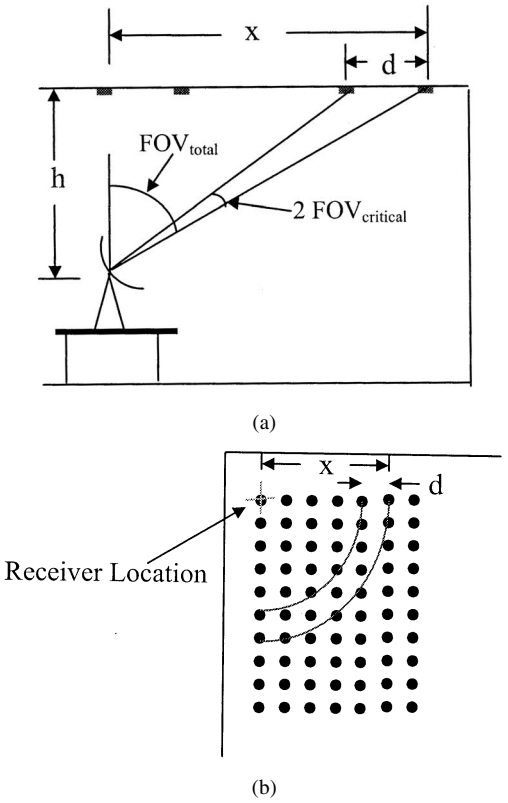

Fig. 6. (a) Illustration of $\mathrm{FOV_{critical}}$ calculations. (b) Top view showing diffusing spots, receiver location, and distance to the farthest spot within the $\mathrm{FOV_{total}}$.

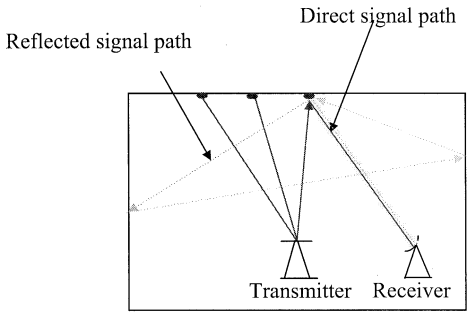

Fig. 7. Illustration of multipath phenomenon caused by multiple reflections.

Thus, in this case, the channel can no longer be modeled as an ideal (dispersion-free) one. Instead, the channel-impulse response is composed of a strong component resulting from the direct path and weaker reflected components. The diversity receiver task is to add a delay to each channel in order to align their strong components, such that the resultant equivalent impulse response $h_{\mathrm{eq}}(t)$ has a strong component at time t_S. The $h_{\mathrm{eq}}(t)$, as shown in Fig. 8, can be expressed as

$$h_{\mathrm{eq}}(t) = \sum_{l=1}^{L} h_l(t) = \sum_{i=-m}^{n} h_i\delta(t - i\Delta - t_S) \tag{29}$$

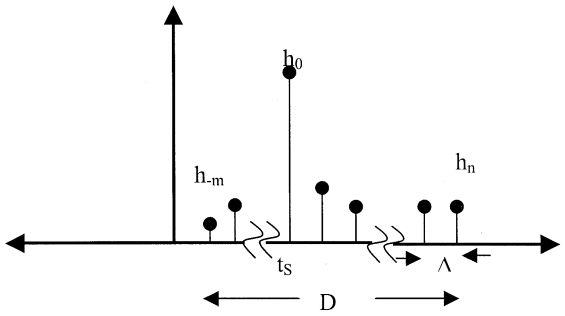

Fig. 8. Equivalent impulse response ($h_{\rm eq}(t)$) of L combined channels.

where $\Delta = (D/(n+m))$ is the sampling time, D is the delay spread, h_l is the shifted impulse response of lth channel, and $h_0 > h_i, \forall i \neq 0$. The $h_{\rm eq}$ is composed of $n+m+1$ impulses. Since some signals will travel shorter and others longer distances than direct path, m impulses precedes h_0 and n will succeed it. For example, when three diffusing spots, of different distances from the receiver, are within an $\mathrm{FOV_{branch}}$, there will be three components in the channels' impulse response. If the middle component is the strongest, the receiver will align this component with the strong components from other branches. The impulse response will contain a component preceding and another succeeding the strong component. The signal at the receiver output, for a single transmitted symbol a_k, is

$$\begin{aligned} y(t) &= \mathrm{RP} a_k f(t) \otimes h_{\rm eq}(t) \otimes g(t) \\ &= \mathrm{RP} a_k x_{rc}(t) \otimes h_{\rm eq}(t). \end{aligned} \tag{30}$$

Using (29) to substitute for $\mathrm{h_{eq}(t)}$, we obtain

$$y(t) = \mathrm{RP} \sum_{i=-m}^{n} a_k h_i x_{rc}(t - i\Delta - t_S - kT). \tag{31}$$

When an infinitely long sequence of symbols is transmitted, the resultant $y(t)$ becomes

$$y(t) = \mathrm{RP} \sum_{k=-\infty}^{\infty} \sum_{i=-m}^{n} a_k h_i x_{rc}(t - kT - i\Delta - t_S). \tag{32}$$

It can be seen from (32) that the receiver output suffers from intersymbol interference (ISI) caused by the residual temporal dispersion. This ISI degrades receiver performance and results in a higher probability of bit error.

V. Performance Measures

In deriving performance measures, two receiver circuits are considered. In the first, the receiver does not account for residual temporal dispersion and samples the kth symbol at $t_{\rm sampling} = kT + t_S$. In the second, the receiver is aware of residual temporal dispersion and therefore tries to optimize the sampling time to minimize the resulting ISI. The receiver in this case samples $y(t)$ at $t_{\rm sampling} = kT + t_S + \delta$, where δ is chosen to minimize ISI. We will refer to these receivers as suboptimal timing circuit and optimal timing circuit receivers, respectively.

A. Receiver With Suboptimal Timing Circuit

In a suboptimal timing circuit receiver, output is sampled without regard to the residual dispersion, i.e., δ is set to zero. Since $x_{rc}(nT) = 0, \forall n \neq 0$ and $x_{rc}(0) = 1$, at sampling time $t_{\rm sampling} = kT + t_S$, the receiver output $y[k]$ is

$$\begin{aligned} y[k] = y[kT] &= \mathrm{RP} a_k h_0 \\ &\quad + \mathrm{RP} \sum_{j=-\infty}^{\infty} \sum_{\substack{i=-m \\ i\neq 0}}^{n} a_j h_i x_{rc}(kT - jT - i\Delta). \end{aligned} \tag{33}$$

The second term in (33) can be decomposed into two components as

$$\begin{aligned} &\mathrm{RP} \sum_{j=-\infty}^{\infty} \sum_{\substack{i=-m \\ i\neq 0}}^{n} a_j h_i x_{rc}\left((k-j)T - i\Delta\right) \\ &\quad = \mathrm{RP} a_k \sum_{\substack{i=-m \\ i\neq 0}}^{n} h_i x_{rc}(-i\Delta) \\ &\qquad + \mathrm{RP} \sum_{\substack{j=-\infty \\ j\neq k}}^{\infty} \sum_{\substack{i=-m \\ i\neq 0}}^{n} a_j h_j x_{rc}\left((k-j)T - i\Delta\right). \end{aligned} \tag{34}$$

The first term shows the effect of channel dispersion on the detected symbol. In other words, if a single symbol is transmitted, this term represents the contribution by channel dispersion to the sampled value $y[k]$. This contribution reduces error probability as long as $\max(i\Delta)$ is less than T. The second term in (34) is the ISI caused by other transmitted symbols. The evaluation of (34) can be simplified by defining an end-to-end impulse response $x(t)$ as

$$x(t) = R x_{rc}(t) * h_{\rm eq}(t) = \mathrm{RP} \sum_{i=-m}^{n} h_i x_{rc}(t - i\Delta) \tag{35}$$

where $x(t)$ represents the response of the equivalent channel to the input $x_{rc}(t)$ scaled by the RP. Expressing $y[k]$ in terms of $x(t)$, we obtain

$$y[k] = a_k x(0) + \sum_{\substack{j=-\infty \\ j\neq k}}^{\infty} a_j x\left((k-j)T\right). \tag{36}$$

When calculating the effect of ISI on the detected symbol, $x(t)$ is recognized as a decaying function. Therefore, the detected symbol is only affected by its neighboring symbols. In this study, the effect of symbols farther than $\pm 6T$ is negligible. Mathematically, this is expressed as

$$x(iT) \approx 0, \quad i = \pm 7, 8, \ldots, \infty. \tag{37}$$

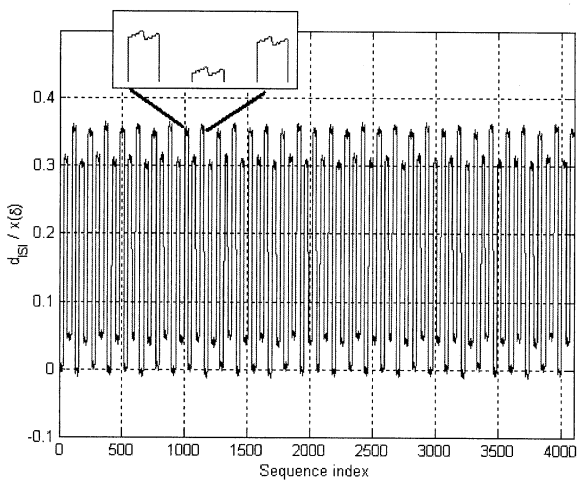

Fig. 9. ISI contribution versus sequence index. The repetition of the pattern indicates that sufficient sequence length is considered in ISI computations.

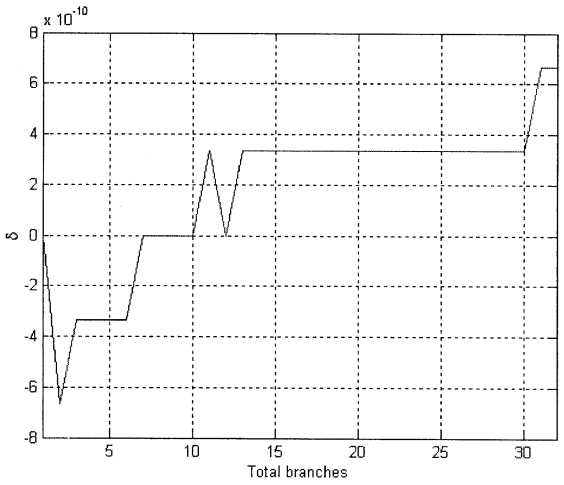

Fig. 10. Timing offset factor δ (s) versus the total number of branches.

The expression for $y[k]$ simplifies to

$$y[k] = a_k x(0) + \sum_{\substack{i=-6 \\ i\neq 0}}^{6} a_{k-i} x(iT). \tag{38}$$

The effect of ISI depends upon the value of the neighboring symbols. Since these symbols are equally likely to be 0 or 1, there are 2^{12} possible neighboring sequences. The ith sequence $\text{seq}_i = [a_{-6}, \ldots a_{-1}, a_1, \ldots, a_6]$ has a decimal equivalent equal to i. The ISI contribution of a sequence $d_{\text{ISI}}(i)$ is given by

$$d_{\text{ISI}}(i) = d_{\text{ISI}}(\text{seq}_i) = \frac{1}{x(0)} \sum_{\substack{j=-6 \\ j\neq 0}}^{6} a_j x(jT) \tag{39}$$

where a_j is chosen from the entries of ith sequence. Fig. 9 shows d_{ISI} as a function of i, for a receiver located in the middle of the room. Two observations are made with regard to the figure. First, the repetition in the pattern every i equal to 512, i.e., d_{ISI} of seq_i and seq_{i+512} are approximately equal. This indicates that $\times$(4T), $\times$(5T), and $\times$(6T) plays insignificant role in determining d_{ISI}. Second, neighboring sequences have approximately equal d_{ISI}, i.e., a_{-6} and a_{-5} values have negligible effect on d_{ISI}. These observations confirm that sufficient sequence length is considered in evaluating d_{ISI}.

Average probability of error is calculated by averaging the conditional probability of error on each sequence. For the ith sequence, an error occurs if $x(0)d_{\text{ISI}}(i)$ and noise exceed a threshold value V_T, i.e.,

$$\begin{aligned} P(e|\text{seq}_i) &= P\left(x(0)d_{\text{ISI}}(i) + \eta > V_T\right) \\ &= Q\left(\frac{V_T - x(0)d_{\text{ISI}}(i)}{\sigma}\right) \end{aligned} \tag{40}$$

where $V_T = (x(0)/2)$. The probability of error is given by

$$P_e = \sum_{i=1}^{2^{2\times 6}} P(e|\text{seq}_i) P(\text{seq}_i). \tag{41}$$

Since the noise is a zero-mean Gaussain process and all sequences are equally likely, the average P_e can be expressed as

$$P_e = \frac{1}{2^{2\times 6}} \sum_{i=1}^{2^{2\times 6}} Q\left(\frac{\frac{x(0)}{2} - x(0)d_{\text{ISI}}(i)}{\sigma}\right). \tag{42}$$

The SNR is defined as

$$\text{SNR} = \frac{x(0)^2}{\sigma^2}. \tag{43}$$

Expressing the average probability of error in terms of SNR, we obtain

$$P_e = \frac{1}{2^{2\times 6}} \sum_{i=1}^{2^{2\times 6}} Q\left[\sqrt{\text{SNR}}\left(\frac{1}{2} - d_{\text{ISI}}(i)\right]\right. . \tag{44}$$

B. Receiver With Optimal Timing Circuit

The receiver with optimal timing circuit chooses a sampling time to reduce the effect of ISI resulting from residual temporal dispersion. In principle, the optimal sampling time $t_{\text{sampling}} = t_S + \delta + kT$ is found by selecting a δ that maximizes the cost function C_{ISI}, defined as

$$C_{\text{ISI}}(\delta) = \frac{1}{2^{2\times 6}} \sum_{i=1}^{2^{2\times 6}} \frac{x(\delta)}{\sum\limits_{\substack{j=-6 \\ j\neq 0}}^{6} a_j^i x(\delta + jT)}. \tag{45}$$

In order to simplify the calculation, we choose the value of δ that maximizes the summand of (45) for the particular sequence. $[a_{-6}, \ldots, a_{-1}, a_1, \ldots, a_6] = [1, 1, \ldots, 1]$. Maximizing C_{ISI} is equivalent to reducing ISI effect on the detected symbol. The value of δ depends on the number of branches and the receiver location. Fig. 10 shows δ as a function of the total number of branches for a given location.

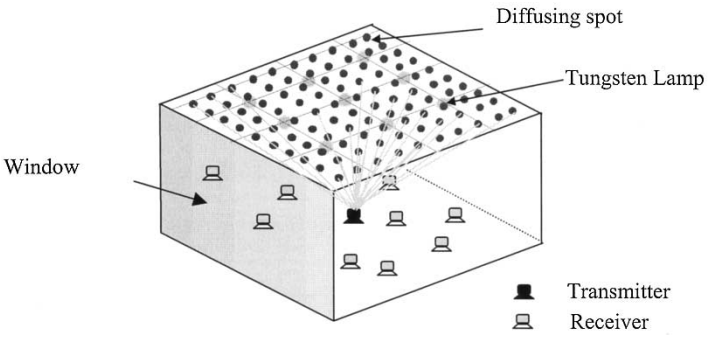

Fig. 11. View of the room used in the computer simulations. Diffusing spots and the Tungsten lamps are shown on the ceiling. The window covers one side of the room.

TABLE II
PARAMETER VALUES USED IN THE COMPUTER SIMULATIONS

Parameter	Value
Room dimensions	(6m, 6m, 3m)
Reflection coefficients of:	
Walls	0.7
Ceiling	0.7
Window	0.04
Floor	0.2
Tungsten lamps	9 lamps located at distances equal to 1.5m apart. The corner lamp is located at (1.5,1.5)
Lamps spectral density	0.037 W/nm [8]
Window	As shown in Figure-11
Diffused solar radiation	8.316 W/m^2 [22]
Spectral range	750 - 950 nm
Receiver locations	400 locations, 0.3m apart, at a fixed height equal to 0.9 m
Receiver FOV$_{branch}$	11.5^o
Photo-detector responsivity	0.6 A/W
Area	1 cm^2
Average transmitted power per spot	0.02W
Bit rate	200 Mbps
Target Average BER	10^{-9}
Impulse Response	3 reflections are considered, Δ=0.33ns, and D=0.1 μs

The expression for P_e is similar to that in (44), with $x(0)$ replaced by $x(\delta)$ and $V_T = (x(\delta)/2)$. Thus, the average probability of error is

$$P_e = \frac{1}{2^{2\times 6}} \sum_{i=1}^{2^{2\times 6}} \left[Q\left(\frac{\frac{x(\delta)}{2} - d_{\mathrm{ISI}}(i,\delta)}{\sigma} \right) \right. \tag{46}$$

where the $d_{\mathrm{ISI}}(i)$ is given by

$$d_{\mathrm{ISI}}(i,\delta) = d_{\mathrm{ISI}}(\mathrm{seq}_i) = \frac{1}{x(\delta)} \sum_{\substack{j=-6 \\ j\neq 0}}^{6} a_j x(\delta + jT). \tag{47}$$

The SNR for the receiver with optimum timing is defined as

$$\mathrm{SNR} = \frac{x(\delta)^2}{\sigma^2} \tag{48}$$

and the probability of error, in terms of SNR, is given by

$$P_e = \frac{1}{2^{2\times 6}} \sum_{i=1}^{2^{2\times 6}} Q\left[\sqrt{\mathrm{SNR}} \left(\frac{1}{2} - d_{\mathrm{ISI}}(i) \right] . \right. \tag{49}$$

VI. SIMULATION RESULTS

In the computer simulations, we considered a room that resembles a typical computer laboratory. The room has dimensions of 6 m × 6 m × 3 m with one of the walls covered by a window, as illustrated in Fig. 11. The transmitter is placed in the center of the room at a height equal to 0.9 m to produce 10 × 10 equally spaced diffusing spots of equal intensity on the ceiling. The technique in [21] is adopted for efficient calculation of channel impulse responses. Three reflections are considered in all impulse response evaluations.

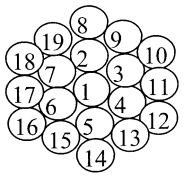

Fig. 12. Branch numbering: branches are added in rings around a central branch and are numbered sequentially.

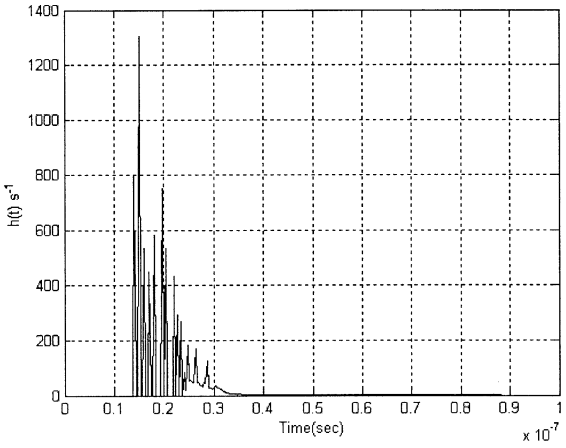

(a)

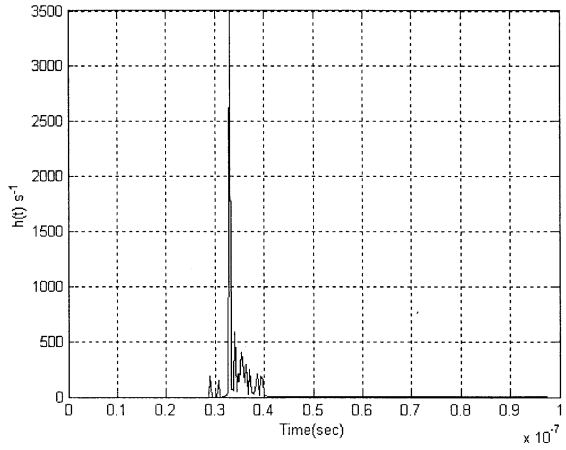

(b)

Fig. 13. (a) Typical impulse response for a single-branch receiver. (b) Impulse response of a multibranch angle-diversity receiver with 32 branches. Both receivers have the same $\mathrm{FOV}_{\mathrm{total}}$ equal to 82.5°.

The receiver has a $\mathrm{FOV}_{\mathrm{branch}} = 11.5°$, which guarantees that at least one diffusing spot is within the $\mathrm{FOV}_{\mathrm{branch}}$ [9]. The total number of branches is chosen such that $\mathrm{FOV}_{\mathrm{total}}$ is less than 90°. A list of parameters used in this simulation is provided in Table II. Error probability, SNR, and outage probability are calculated as a function of total number of receiver diversity branches. The central branch is labeled as 1. Subsequent branches are numbered in an increasing order as they move away from the central branch, as illustrated in Fig. 12. The impulse responses of the channel with a single-branch and angle-diversity receiver are shown in Fig. 13, parts (a) and (b), respectively. This figure demonstrates the multibranch receiver ability to reduce temporal dispersion.

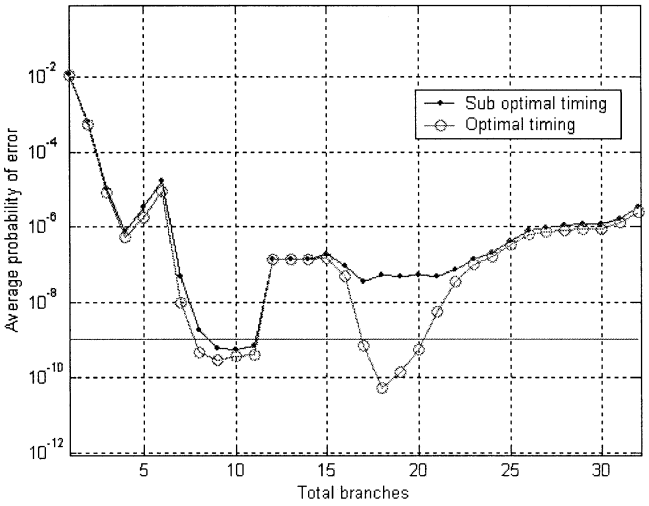

Fig. 14. Average probability of error for 400 receiver locations.

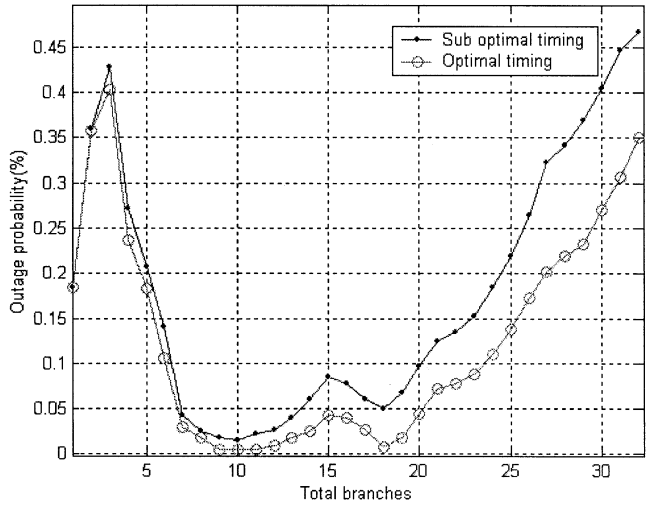

Fig. 15. Outage probability defined by the percentage of locations that correspond to an error probability greater than 10^{-9}.

The receiver performance is evaluated at 400 different locations. The distance between two locations is 0.3 m; this ensures that performance can be attained throughout the room by moving a receiver a maximum distance less than or equal to 0.3 m. Fig. 14 shows the average probability of error for 400 locations as a function of the total number of branches. From the figure, an average probability of error equal to 10–9 (shown as a horizontal line) is achieved by 8 and 9 branches for a receiver using optimal and suboptimal timing circuit, respectively. An increasing number of branches beyond 11 increases P_e for a suboptimal timing receiver. The optimal timing receiver achieves a minimum average P_e with 18 branches.

Although average error probability provides some insight regarding the link performance, a more meaningful measure is achieved using outage probability. This is true since, with a large number of receiver locations considered, few locations that fall within high exposure of ambient light might result in a small average error probability. Outage probability is defined as a percentage of locations that fail to meet the 10^{-9} threshold P_e re-

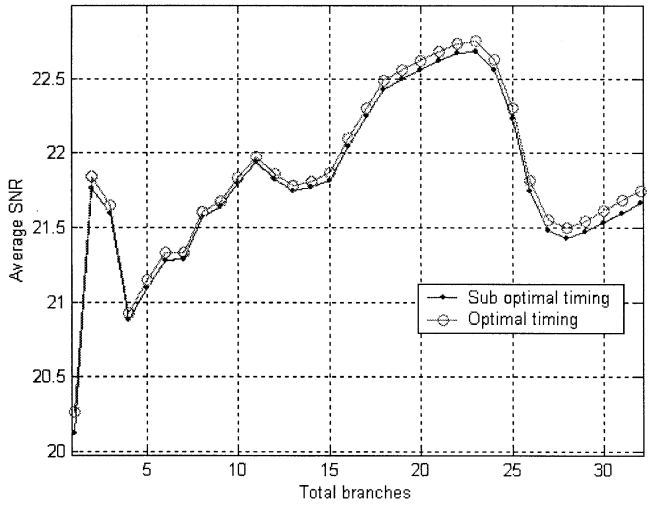

Fig. 16. Average SNR versus total number of branches.

quirement, for a given number of branches. The plot of outage probability in Fig. 15 shows that minimum outage probabilities of 0.5% and 1.5% are achieved using nine and ten branches for receivers employing optimal and suboptimal timing circuits, respectively.

The average SNR is plotted in Fig. 16. This figure shows the variation in the average SNR as new branches are added. The maximum average SNR is achieved with 23 branches. It is interesting to note that this number of branches does not correspond to a minimum average error probability. This is the case since the SNR calculation does not account for the ISI effect.

VII. Conclusion

Indoor wireless IR transmissions tend to suffer with multipath temporal dispersion caused by the different path lengths traveled by scattered light rays. This paper demonstrates that angle diversity at the receiver is an effective technique to reduce channel dispersion effect, in turn reducing the ISI and the error probability. In designing an angle-diversity receiver, three parameters must be specified: $\mathrm{FOV}_{\mathrm{total}}$, $\mathrm{FOV}_{\mathrm{branch}}$, and the total number of branches. The choice of $\mathrm{FOV}_{\mathrm{branch}}$ depends on the pattern of diffusing spots, their separation distances, and the distance between the receiver and spots region. A tradeoff is needed in choosing the $\mathrm{FOV}_{\mathrm{branch}}$. Reducing the $\mathrm{FOV}_{\mathrm{branch}}$ enhances the receiver ability to combat temporal dispersion, but it also reduces the branch ability to capture diffusing spots. The choice of number of branches depends on the noise level and the relative contribution of the new added branches. It has been demonstrated through evaluation of outage probability that there exists an optimal number of branches that achieves the desired performance requirements. The number is optimal in the sense that it is the smallest number of branches that enable achieving a desired set of performance requirements. This, in turn, reduces the receiver cost, complexity, and susceptibility to shadowing effect that occurs when an obstacle blocks signals' path. The impact of using optimal timing circuit at receivers is insignificant when the $\mathrm{FOV}_{\mathrm{branch}}$ is small. This is because the channel impulse response up to these branches contains at most one strong component, which can be aligned by the receiver. As $\mathrm{FOV}_{\mathrm{branch}}$ increases, the channel impulse response for some branches contain two or more strong components and the receiver is only able to align one. Thus, the timing circuit plays a more significant role in reducing the ISI in this case. The improvement using timing circuit becomes less significant as the number of branches increases, because the added branches contribute a weaker signal, considering their position and distance.

References

[1] J. R. Barry, *Wireless Infrared Communications*. Norwell, MA: Kluwer, 1994.

[2] G. Yun and M. Kavehrad, "Spot diffusing and fly-eye receivers for indoor infrared wireless communications," in *Proc. IEEE Int. Conf. Selected Topics in Wireless Communications*, Vancouver, BC, Canada, June 1992, pp. 262–265.

[3] E. Simova and M. Kavehrad, "Light shaping diffusers for indoor wireless infrared communications via a holographic approach," in *Proc. SPIE Photonics West'96*, San Jose, CA, Feb. 1996.

[4] E. Simova, M. Tai, and M. Kavehrad, "Indoor wireless infrared link with a holographic multiple-spot diffuser," in *Proc. ICAPT*, Montreal, QC, Canada, Aug. 1996.

[5] R. T. Valadas and A. M. de Oliveira Duarte, "Sectored receivers for indoor wireless optical communication systems," in *Proc. IEEE 5th Int. Symp. Personal, Indoor, and Mobile Radio Communications*, vol. 4, Joint PIMRC'94/WCN—Proc., The Hague, The Netherlands, Sept. 18–22, 1994, pp. 1090–1095.

[6] J. B. Carruthers and J. M. Kahn, "Angle diversity for nondirected wireless infrared communication," *IEEE Trans. Commun.*, vol. 48, pp. 960–969, June 2000.

[7] S. Jivkova and M. Kavehrad, "Indoor wireless infrared local access, multi-spot diffusing with computer generated holographic beam-splitter," in *Proc. ICC'99*, Vancouver, BC, Canada, June 1999.

[8] ——, "Multi-spot diffusing configuration for wireless infrared access," *IEEE Trans. Commun.*, vol. 48, pp. 970–978, June 2000.

[9] K. Akhavan, M. Kavehrad, and S. Jivkova, "Wireless infrared in-house communications: how to achieve very high bit rates," in *Proc. IEEE WCNC 2000*, Chicago, IL, Sept. 2000.

[10] W.-C. Jeong, M. Kavehrad, and S. Jivkova, "Broadband infrared access with a multi-spot diffusing configuration: performance," *Int. J. Wireless Inform. Networks*, vol. 8, no. 1, 2001.

[11] S. Jivkova and M. Kavehrad, "Holographic optical receiver front-end for wireless infrared indoor communications," *OSA Appl. Opt. J.*, June 2001.

[12] ——, "Receiver designs and channel characterization for multispot high bit rate wireless infrared communications," *IEEE Trans. Commun.*, vol. 49, pp. 2145–2153, Dec. 2001.

[13] K. Akhavan, M. Kavehrad, and S. Jivkova, "High-speed power-efficient indoor wireless infrared communication using code combining, part II," *IEEE Trans. Commun.*, vol. 50, pp. 1495–1502, Sept. 2002.

[14] ——, "High-speed power-efficient indoor wireless infrared communication using code combining, part I," *IEEE Trans. Commun.*, vol. 50, pp. 1098–1109, July 2002.

[15] S. Jivkova, S. Shurulinkov, and M. Kavehrad, "Holographic parabolic mirror as a receiver optical front-end for wireless infrared communications: experimental study," *Appl. Opt. J.*, Sept. 2002.

[16] P. Djahani and J. M. Kahn, "Analysis of infrared wireless links employing multi-beam transmitters and imaging diversity receivers," *IEEE Trans. Commun.*, vol. 48, pp. 2077–2088, Dec. 2000.

[17] G. P. Agrawal, *Fiber-Optic Communication Systems*. New York: Wiley, 1997.

[18] S. B. Alexander, *Optical Communication Receiver Design*. Bellingham, WA: SPIE, 1997.

[19] J. G. Proakis, *Digital Communications*. New York: McGraw-Hill, 1995.

[20] J. Anderson, *Digital Transmission Engineering*. Englewood Cliffs, NJ: Prentice-Hall, 1998.

[21] Y. Alqudah and M. Kavehrad, "Assessing the feasibility of new diffused configuration for broadband wireless infrared links," in *Proc. IEEE WCNC'03*, New Orleans, LA, Mar. 2003.

[22] W. Marion and S. Wilcox, *Solar Radiation Data Manual for Buildings*: Nat. Renewable Energy Lab., 1995.

Yazan A. Alqudah was born on August 3, 1971, in Ajloun, Jordan. He received the B.S degree in electrical engineering from the University of Jordan, Yarmouk, in 1993, the B.S. degree in electrical engineering from The Pennsylvania State University (Penn State), College Park, in 1997, and is currently working toward the Ph.D. degree at Penn State.

After graduation, he was a Laboratory Instructor at Yarmouk University. During his studies toward the M.S. degree, he was a Teaching Assistant, where he assisted with the design and building of experiments for the digital control laboratory. His M.S. thesis work investigated using feedback control to reduce motion artifacts in magnetic resonance imaging (MRJ). In 1997, he joined Schlumberger, PA, as part of his practical training. He was an Applications and Software Engineer. During his assignments, he was responsible for the personalization of subscriber identity modules (SIM) and over-the-air customization services for GSM carriers in North America. He received teaching and research assistantship positions at Penn State's Electrical Engineering Department. His current research interests include communication systems, channel modeling, and broad-band optical wireless communication.

Mohsen Kavehrad (S'75–M'78–SM'86–F'92) received the Ph.D. degree in electrical engineering from the Polytechnic University (Brooklyn Polytechnic), Brooklyn, NY, in 1977.

He was with Fairchild Industries (Space Communications Division) and GTE (Satellite Corporation and Laboratories) between 1978 and 1981. In December 1981, he joined Bell Laboratories. In March 1989, he joined the Department of Electrical Engineering, University of Ottawa, Ottawa, ON, Canada, as a Full Professor, where he was at the same time the Director of the Broadband Communications Research Laboratory. He was also Director of the Photonic Networks and Systems Thrust and a Project Leader in the Communications and Information Technology Ontario (CITO), Ottawa, and the Director of Ottawa-Carleton Communications Center for Research (OCCCR), Ottawa. In January 1997, he joined the Department of Electrical Engineering, The Pennsylvania State University (Penn State), College Park, as the W. L. Weiss (AMERITECH) Professor of Electrical Engineering and the Director of Communications Engineering and, later, in August 1997, he was appointed as the Founding Director of the Center for Information and Communications Technology Research (CICTR). From 1997 to 1998, he was also the CTO and a Vice President at Tele-Beam Inc., State College, PA. His research interests are in the areas of technologies, systems, and network architectures that enable the vision of the information age, e.g., broad-band wireless communications systems and networks and optical fiber communications systems and networks. His works have been published in over 270 refereed journal and conference papers, several book chapters, and books. He holds several key issued patents in these areas.

Dr. Kavehrad has lectured worldwide as an IEEE Distinguished Lecturer and as plenary and keynote speaker at leading conferences. He has received three Exceptional Technical Contributions Awards while he was with Bell Laboratories, for his work on wireless communications systems. In 1990, he received the TRIO Feedback Award for his patent on a "Passive Optical Interconnect." He also received the 2001 IEEE VTS Neal Shepherd Best Propagation Paper Award and three IEEE Lasers and Electro-Optics Society Best Paper Awards and a Canada NSERC Ph.D. dissertation award, jointly with his former graduate students for their works on wireless and optical systems.